

Relativistic distorted-wave analysis of the missing-energy spectrum measured with monochromatic ν_μ - ^{12}C interactions at JSNS²

J. M. Franco-Patino,¹ M. B. Barbaro,^{2,3} and G. Co' ^{1,4}

¹*INFN Sezione di Lecce, Via Arnesano, I-73100 Lecce, Italy*

²*Dipartimento di Fisica, Università di Torino, Via P. Giuria 1, 10125 Torino, Italy*

³*INFN, Sezione di Torino, Via Pietro Giuria 1, 10125 Torino, Italy*

⁴*Dipartimento di Matematica e Fisica “E. De Giorgi”, Università del Salento, I-73100 Lecce, Italy*

(Dated: March 4, 2026)

Recently, the JSNS² collaboration measured for the first time the missing-energy distribution of ^{12}C using a monochromatic neutrino beam coming from kaon decays at rest. In this work we present the results of an analysis of this spectrum using the relativistic distorted-wave approach with a new parameterization of the spectral function for neutrons in ^{12}C , which incorporates detailed information from $(e, e'p)$ experiments with high missing-energy resolution. The role of the recoil of the residual nucleus in the description of the measured distribution, final-state interactions, and the ability of neutrino event generators to describe low-energy nuclear effects are discussed.

I. INTRODUCTION

Motivated by the global effort to measure the neutrino-oscillation parameters, neutrino-nucleus interactions have been investigated with unprecedented intensity [1]. The interpretation of accelerator-based measurements requires accurate modeling of neutrino-nucleus cross sections over a wide range of energies. Since neutrino beams are commonly produced via charged-particle decays in flight, they exhibit a broad energy spectrum at the detector, which complicates the reconstruction of the incident neutrino energy on an event-by-event basis. Moreover, beyond the intrinsic uncertainties in energy reconstruction, determining the reaction mechanism underlying the measured observables remains a persistent and nontrivial challenge.

Kaon decays at rest (KDAR) provide a unique opportunity to study neutrino-nucleus interactions while avoiding the complications associated with neutrinos produced by meson decays in flight. The resulting monoenergetic ν_μ beam, with $E_\nu = 235.5$ MeV, constitutes an especially clean probe for the direct study of nuclear effects such as initial- and final-state interactions and correlations in the nuclear medium. More broadly, KDAR ν_μ offer the prospect of substantially reducing experimental and theoretical uncertainties and mitigating longstanding ambiguities.

Although KDAR neutrinos were observed for the first time by the MiniBooNE collaboration [2], the JSNS² collaboration [3] has set a new paradigm in neutrino physics. For the first time, in a laboratory scattering experiment, the missing-energy spectrum of neutrons in ^{12}C using KDAR neutrinos was measured. Unfortunately, only the shape of the cross section versus the missing energy is available and not its normalization. Despite of this limitation, these first data represent an important step forward in the direction of understanding the low-energy neutrino-nucleus interaction.

In this article, we present the results of an investigation aimed to study the role played by various nuclear

effects related to the neutrino-nucleus interaction. We start by using the relativistic-mean field model [4–6] to describe the nucleus ground-state. We correct this basic model by adding effects beyond the mean-field approximation based on a parameterization of the ^{12}C spectral function given in [7]. For the modeling of final-state interactions, we include proton distortion using the relativistic distorted-wave formalism [8–14] and simulate the inelastic interactions using the neutrino event generator NuWro [15, 16].

In Sec. II we summarize the general kinematics of the interaction of a monochromatic neutrino with a nucleus in the impulse approximation. In Sec. III and Sec. IV we address the relativistic distorted-wave formalism, as well as the description of the ground-state nucleus within the relativistic-mean model with a parameterized spectral function. In Sec. V we present a comparison of the JSNS² measurement and the theoretical predictions. Finally, we draw our conclusions in Sec. VI.

II. KINEMATICS

We present in this section the basic expressions of our description of the process studied by the JSNS² collaboration where muon neutrinos generated by the KDAR process impact on the ^{12}C target inducing a charge current (CC) reaction producing a μ^- of energy E_μ . We will be working under the assumption that, given the low energy of the incoming neutrino, the main interaction channel is the quasielastic (QE) scattering off a single bound neutron in ^{12}C . This means that the value of the energy transferred to the bound neutron $\omega = E_\nu - E_\mu$ is above the nucleon emission threshold. Therefore, our final state will be characterized by a residual nucleus B and one proton emitted with energy E_p . The residual nucleus of mass M_B has total energy E_B which includes the recoil kinetic energy T_B and an eventual excitation energy ξ , such as $E_B = M_B + T_B + \xi$.

In the laboratory frame, with the z axis aligned with

the incoming neutrino momentum \mathbf{k}_ν , and within the impulse approximation (IA), where the exchanged W

boson is assumed to couple to a single bound nucleon that is subsequently ejected, the semi-inclusive $\nu_\mu + A \rightarrow \mu + p + B$ cross section can be written as [13]

$$\frac{d\sigma(E_\nu)}{dk_\mu d\Omega_\mu dp_p d\Omega_p dE_m} = \frac{G_F^2 \cos^2 \theta_c k_\mu^2 p_p^2}{64\pi^5} L_{\mu\nu} H^{\mu\nu} \delta(\omega + M_A - E_p - E_B), \quad (1)$$

where \mathbf{k}_μ , \mathbf{p}_p denote the momenta of the ejected muon and proton, respectively, and Ω_μ and Ω_p represent their corresponding emission angles. We indicate with M_A is the mass of the target nucleus, with G_F the Fermi constant and with θ_c the Cabibbo angle. The cross section is also a function of the contraction of the leptonic $L_{\mu\nu}$ and the hadronic $H^{\mu\nu}$ tensors.

The observable measured by JSNS², the missing energy E_m , is defined as follows

$$E_m = E_s^n + \xi = M_B - M_A + m_n + \xi, \quad (2)$$

where $E_s^n = M_B - M_A + m_n$ is the neutron separation energy. The energy conservation in Eq. (1) can be expressed as

$$\omega + M_A = E_p + E_B \longrightarrow \omega + m_n = E_m + T_p + m_p + T_B, \quad (3)$$

where m_p is the mass of the emitted nucleon, T_p its kinetic energy, and T_B is the kinetic energy of the residual nucleus

$$T_B = E_B - M_B - \xi = \sqrt{\mathbf{p}_m^2 + (M_B + \xi)^2} - M_B - \xi. \quad (4)$$

We indicate with $\mathbf{p}_m = \mathbf{p}_p - \mathbf{q}$ the missing momentum, which is fixed by momentum conservation and depends on the momentum of the ejected nucleon \mathbf{p}_p and on the transferred momentum $\mathbf{q} = \mathbf{k}_\nu - \mathbf{k}_\mu$.

The recoil of the residual nucleus T_B in Eq. (3) introduces a complicated angular dependence in the energy-conservation delta function, making the integration over one of the variables in Eq. (1) non-trivial. For instance, if we solve the energy conservation to integrate on p_p we obtain a quadratic equation

$$[A_0^2 - \alpha^2] p_p^2 - \alpha \Delta p_p + A_0^2 m_p^2 - \Delta^2/4 = 0, \quad (5)$$

where

$$\begin{aligned} A_0 &= E_\nu - E_\mu + M_A \\ \Delta &= A_0^2 + m_p^2 - q^2 - (M_B + \xi)^2 \end{aligned} \quad (6)$$

$$\alpha = E_\nu \cos \theta_p - k_\mu (\sin \theta_\mu \sin \theta_p \cos \phi_p + \cos \theta_\mu \cos \theta_p).$$

Integrating over p_p using the delta function introduces a factor

$$f_{\text{rec}}^{-1} = \left| \frac{p_p}{E_p} + \frac{p_p - \alpha}{E_B} \right|^{-1},$$

in the expression of the cross section. Then, Eq. (1) becomes

$$\frac{d\sigma(E_\nu)}{dk_\mu d\Omega_\mu d\Omega_p dE_m} = \frac{G_F^2 \cos^2 \theta_c k_\mu^2 p_p^2}{64\pi^5 f_{\text{rec}}} L_{\mu\nu} H^{\mu\nu}, \quad (7)$$

where p_p is the solution of Eq. (5). If the two solutions of Eq. (5) are valid, then the cross section is the incoherent sum of both solutions. As we will show later, retaining the recoil of the residual nucleus in Eq. (3) allows us to investigate its impact on the missing-energy spectrum measured by JSNS².

III. THE RELATIVISTIC DISTORTED-WAVE APPROACH

The kinematic region accessible to the JSNS² experiment requires a careful treatment of nuclear effects (*e.g.* Pauli blocking, ground state correlations, re-interaction of the emitted nucleon with the residual nucleus, etc.) in order to accurately describe the experimental results [17].

In this work we adopt the relativistic distorted-wave approach based on the energy dependent-relativistic mean field model (ED-RMF) [18, 19]. This model has been used to describe inclusive (e, e') data that overlaps in phase-space with 235.5 MeV ν_μ scattering processes [18].

In our description of the process we consider that ν_μ interacts with a bound neutron which becomes a proton because of the CC weak interaction. The proton is then emitted from the nucleus. In our model, the remaining nucleons act as inert spectators in the one-body process described above. In the relativistic distorted-wave impulse approximation (RDWIA) we can express the hadronic tensor $H^{\mu\nu}$ of Eq. (7) as a sum over occupied initial-states identified by the quantum number κ

$$H^{\mu\nu} = \sum_{\kappa} \mathcal{H}_{\kappa}^{\mu\nu} = \sum_{\kappa} \rho_{\kappa}(E_m) \sum_{s_p, m_j} J_{s_p, \kappa, m_j}^{\mu} J_{s_p, \kappa, m_j}^{\nu*}, \quad (8)$$

where the hadronic current is

$$J_{s_p, \kappa, m_j}^{\mu} = \int d\mathbf{r} e^{i\mathbf{r}\cdot\mathbf{q}} \bar{\Psi}^{s_p}(\mathbf{r}, p_p) \hat{j}^{\mu} \Phi_{\kappa}^{m_j}(\mathbf{r}), \quad (9)$$

and $\rho_{\kappa}(E_m)$ indicates the missing energy profile. In the above expressions $j = |\kappa| - 1/2$ is the total angular momentum of the bound neutron, m_j its third component

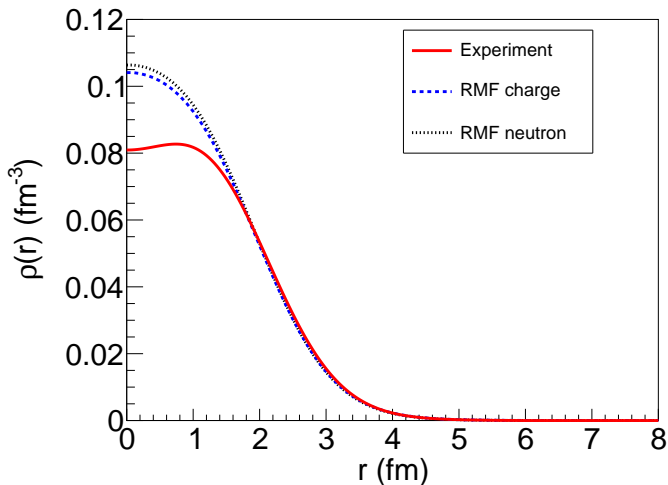


FIG. 1. Charge and neutron radial density calculated with the RMF potential NLSH [20], compared with a fit to elastic electron-nucleus scattering data [21]. The root-mean-square (rms) charge radius obtained with NLSH is 2.46811 fm, in agreement with the experimental value of 2.4701 ± 0.0022 fm [22].

and s_p is the spin projection of the ejected proton. The weak current one-body operator \hat{J}^μ has the CC2 expression given in Ref. [13]. The wave functions Ψ^{s_p} and Φ_κ^{mj} are four-dimensional spinors that describe, respectively, the scattered and bound nucleons.

$$\Psi^{s_p}(\mathbf{r}, p_p) = 4\pi \sqrt{\frac{E_p + m_p}{2E_p}} \sum_{\kappa, \mu, m'} e^{i\delta_\kappa} i^l \langle l m' \frac{1}{2} s_p | j \mu \rangle Y_{lm'}^*(\Omega_p) \psi_\kappa^\mu(\mathbf{r}, p_p), \quad (10)$$

where $Y_{lm}(\Omega_p)$ are the spherical harmonics that describe the direction of the emitted proton and δ_κ is the phase shift obtained by matching the distorted wave-function to the Dirac-Coulomb wave-function. The orbital momentum l is fixed by κ and take the values $l = \kappa$ if $\kappa > 0$ and $l = -\kappa - 1$ if $\kappa < 0$. The wave function $\psi_\kappa^\mu(\mathbf{r}, p_p)$ is a four-component spinor of the form

$$\psi_\kappa^\mu(\mathbf{r}, p_p) = \begin{pmatrix} g_\kappa(E_p, r) \Phi_\kappa^\mu(\Omega_r) \\ i f_\kappa(E_p, r) \Phi_{-\kappa}^\mu(\Omega_r) \end{pmatrix} \quad (11)$$

with the Pauli spin-spherical harmonics

$$\Phi_\kappa^\mu(\Omega_r) = \sum_{s_p} \langle l m_l \frac{1}{2} s_p | j \mu \rangle Y_l^\mu(\Omega_r) \chi^{s_p}, \quad (12)$$

where χ^{s_p} is a Pauli spinor of two components and g_κ and

The ^{12}C ground state is described in terms of single particle wave functions $\Phi_\kappa^{mj}(\mathbf{r})$ obtained within the independent-particle shell model, where the nucleons inside the nucleus occupy discrete energy states that are eigenvalues of a spherically symmetrical potential. For this work, we consider a fully relativistic framework where the bound states are solutions of the Dirac equation with scalar and vector potentials given by the relativistic mean field (RMF) approach [4–6]. The free parameters of the RMF potential are fitted to reproduce different properties of finite nuclei. In this work, we use the potential NLSH described in [20]. Table. I lists the model predictions for the neutron and proton separation energies in ^{12}C , while Fig. 1 shows the corresponding densities and root-mean-square charge radius.

	protons		neutrons	
	th.	exp.	th.	exp.
$1p_{3/2}$	14.46	15.96	17.81	18.72
$1s_{1/2}$	40.50	-	44.37	-

TABLE I. Energy levels of the $1p_{3/2}$ and $1s_{1/2}$ shells obtained with the NLSH parameterization [20] for protons and neutrons in ^{12}C compared with the empirical separation energies from Ref. [23]. All the energies are in MeV.

Within RDWIA, the wave function $\Psi^{s_p}(\mathbf{r}, p_p)$ describes the scattered proton with asymptotic momentum p_p and is given by

f_κ satisfy the following coupled-differential equations

$$\begin{aligned} \frac{df_\kappa}{dr} &= \frac{\kappa - 1}{r} f_\kappa - \left(E_p - m_p - V(r) \right) g_\kappa \\ \frac{dg_\kappa}{dr} &= -\frac{\kappa - 1}{r} g_\kappa + \left(E_p + m_p - V(r) \right) f_\kappa. \end{aligned} \quad (13)$$

Our theoretical predictions for the QE channel will correspond to two calculations based on the distorted-wave approach with two different potentials $V(r)$. One of the models is based on the ED-RMF potential [18, 19], which is real and used to describe inclusive (e, e') and (ν, l) data, and the other is based on the relativistic optical potential (ROP) [24], which is complex and can be used to describe ($e, e'p$) data [8–10]. Notice that there is a third option, which is not realistic for the kinematics involved in the process, that is the relativistic plane-wave model (RPWIA) where the coupled equations are solved with $V(r) = 0$.

IV. MISSING ENERGY PROFILE PARAMETERIZATION

In the extreme mean-field model presented so far, the missing-energy distribution $\rho_\kappa(E_m)$ is given by a sum of Dirac delta functions. These delta functions ensure that the missing energy can take only discrete values, corresponding to the energy eigenvalues of the fully occupied single-particle states given the RMF model. This model is relatively simple, and a meaningful comparison with the missing-energy distribution measured by JSNS² requires a more realistic description of the initial nuclear bound state that incorporates correlations, *i.e.*, effects beyond the pure mean-field approximation.

There is an extensive body of literature addressing microscopic calculations of spectral functions, which lead to the missing-energy profile $\rho_\kappa(E_m)$ [25, 26]. Here, we adopted a phenomenological approach and, building on previous work [11, 13], introduced a new parameterization of the missing-energy profile $\rho_\kappa(E_m)$ for neutrons in ¹²C. The parameterization was based on the updated spectral function of Ref. [7] which was optimized to improve the agreement with exclusive ($e, e'p$) data [27]. The improvement was obtained by modeling the region dominated by the p -states with three Dirac deltas instead of only one narrow Gaussian.

In our modeling of $\rho_\kappa(E_m)$, three distinct contributions are considered. The first contribution is associated with the occupancy of the p -states and corresponds to the energy region extending from the neutron emission threshold to about 22 MeV ($E_m \approx 18$ -22 MeV). In this region, the profile is represented by three Dirac delta functions as in Ref. [7]. Those three p -states correspond to a $1p_{3/2}$ shell describing the ground state and two excited states, namely $1p_{1/2}$ and $1p_{3/2}$, corresponding to 2.125 MeV and 5.020 MeV of excitation energy [27]. For both excited states we use the same wave-function predicted by the RMF model for the $1p_{3/2}$ ground-state.

The second contribution is associated with the s -states, which ($e, e'p$) experiments indicate to exhibit a large width. We abandoned the usual gaussian parameterization in favor of an asymmetric Maxwell-Boltzmann shape of the type

$$\rho_{1s1/2}(E_m) = \frac{4n_{1s1/2}}{\sigma\sqrt{\pi}} \exp\left(-\frac{(E_m-\mu+\sigma)^2}{\sigma^2}\right) \frac{(E_m-\mu+\sigma)^2}{\sigma^2}; \quad (14)$$

with $\mu = 37.0$ MeV and $\sigma = 19$ MeV. In Fig. 2 we compare the missing-energy profiles of a neutron in a s -state obtained using Gaussian and Maxwell-Boltzmann distributions. The two distributions are normalized at the same value, corresponding to $n_{1s1/2} = 1.74$ nucleons. The Maxwell-Boltzmann distribution avoids the unphysical contribution at E_m values below the nucleon emission threshold.

The third contribution in our modeling of $\rho_\kappa(E_m)$ is related to the region of E_m and p_m where the effects of short-range correlations on the spectral function are sig-

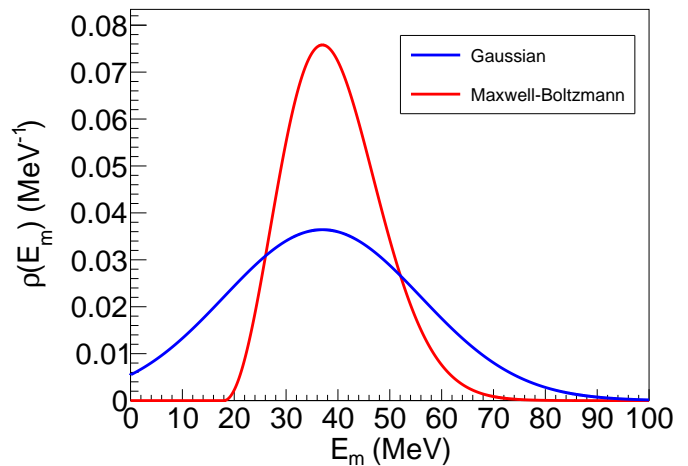


FIG. 2. Missing energy profile of a neutron in a s -state of ¹²C parameterized with $\mu = 37$ MeV and $\sigma = 19$ MeV using Gaussian and Maxwell-Boltzmann distributions (see Eq. (14)). Both distributions are normalized to $n_{1s1/2} = 1.74$ nucleons.

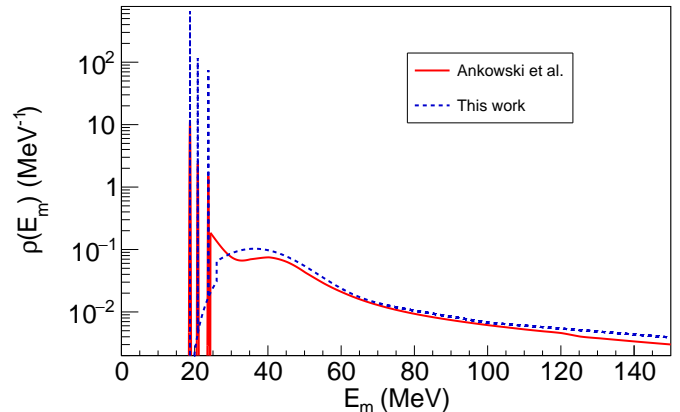


FIG. 3. Comparison of our missing energy profile $\rho_\kappa(E_m)$ of neutrons with that of Ref. [7]. A shift of +2.764 MeV has been applied to the results of Ankowski *et al.* to account for neutron, rather than proton, emission (see text for explanation).

nificant [7]. We refer to this contribution as the “background” and parametrize it as follows to reproduce the high-energy tail reported in [7]:

$$\rho_{\text{backg}}(E_m) = n_b \exp(-x_{\text{cut}}b) \exp\left(-w(E_m - x_{\text{cut}})\right) \quad (15)$$

for $26 < E_m < 100$ MeV, and

$$\rho_{\text{backg}}(E_m) = n_b \exp(-bE_m) \quad (16)$$

for $100 < E_m < 300$ MeV. The parameters values are $n_b = 0.02$, $b = 0.0109$ MeV⁻¹, $w = 0.022$ MeV⁻¹ and $x_{\text{cut}} = 100$ MeV.

Our model for $\rho_\kappa(E_m)$ is obtained by summing these three contributions, each normalized to the occupancy

values listed in Table II. Figure 3 shows a comparison of our $\rho_\kappa(E_m)$ with that of Ref. [7]. The main difference between the two profiles occurs in the region where the contributions of p - and s -shells overlap. This explains the discrepancies between our occupation values and those reported in the $(e, e'p)$ experiments of Refs. [27, 28], as reproduced by Ankowski *et al.* [7]. Also, the distribution has been shifted by +2.764 MeV to account for the fact that we consider neutron emission, whereas Ref. [7] refers to proton emission.

	E_κ (MeV)	n_κ
$1p_{3/2}$	18.724	1.95
$1p_{1/2}$	20.844	0.29
$1p_{3/2}$	23.734	0.22
$1s_{1/2}$	37.0	1.74
background	-	1.80

TABLE II. Energies E_κ and neutrons number n_κ for the different contributions in our modeling of $\rho_\kappa(E_m)$. In the case of the s -state, E_κ denotes the peak position of the Maxwell-Boltzmann distribution.

V. COMPARISON WITH EXPERIMENTAL DATA

The cross-section data reported by the JSNS² collaboration [3] is presented as a function of the missing energy E_m . This quantity, defined in Eq. (2), is reconstructed experimentally using the following expression

$$E_m = E_\nu - m_\mu + m_n - m_p - E_{\text{vis}} \quad , \quad (17)$$

where E_{vis} is the visible energy collected by JSNS² liquid scintillator detector. In the pure QE regime, where only a single proton is emitted, E_{vis} can be obtained using Eq. (3)

$$E_{\text{vis}} = T_\mu + T_p + T_B \quad . \quad (18)$$

This represents a simplified description of the process. Additional effects may modify the value of E_{vis} and, consequently, of E_m ; for example, photons emitted during nuclear de-excitation or neutron emission induced by the re-scattering of the outgoing proton.

We emphasize here an important issue regarding the definition of E_{vis} . In [3] the JSNS² collaboration defines the visible energy without considering T_B , the kinetic energy of the residual nucleus. The experimental report specifies that only the kinetic energies of the charged particles are considered. Additional potential sources of visible energy, including the recoil of the residual nucleus, are not incorporated in the simulation and are therefore not subtracted from the data. Our model allows us to evaluate T_B yielding values up to approximately 5 MeV; this contribution is therefore not negligible. One may question its overall relevance, since the heavy residual

nucleus moves very slowly in the detector and may produce signals below the detection threshold. As this issue remains open, in the following we present theoretical predictions both including and neglecting the recoil contribution when comparing with the experimental data. In this way, we quantify the impact of omitting the recoil term from E_{vis} .

Another important issue concerns neutron emission. This process may occur when the primary proton produced at the interaction vertex by the neutrino undergoes re-scattering inside the nucleus, interacting with a neutron so that both nucleons are emitted. Since neutrons do not generate detectable signals in the detector, the measured value of E_{vis} in Eq. (18) is smaller than that implied by energy conservation. As a result, the reconstructed value of E_m in Eq. (17) is overestimated with respect to its true value. Consequently, events in a E_m bin are shifted toward higher missing-energy bins.

Our RDWIA approach takes into account the distortion of the scattered proton in a quantum-mechanical way, however neither the ED-RMF nor the ROP models are able to simulate the neutron emission. In the ROP approach many effects beyond the single proton emission are effectively considered in the imaginary part of the potential, but it is not possible to identify the neutron emission contribution.

We tackle this problem by employing one-proton emission events generated according to the ED-RMF model as input to a generator's semiclassical cascade. The cascade subsequently redistributes the initial ($1p$) strength into more complex final states, including ($1p1n$), ($1pNn$), ($2p$), etc. This method has been applied [12, 29–31] to benchmark cascade models against ROP predictions, as well as to perform studies and comparisons with other neutrino-nucleus scattering data. In this work, we employ the NuWro [15, 16] intranuclear cascade model to evaluate the effects of inelastic neutron emission in the comparison with the JSNS² missing-energy measurement.

Model	Integrated cross-sections (cm ²)			
	p-shells	s-shell	Background	Total
RPWIA	5.06×10^{-39}	2.87×10^{-39}	6.6×10^{-40}	8.59×10^{-39}
ED-RMF	4.18×10^{-39}	1.89×10^{-39}	4.6×10^{-40}	6.53×10^{-39}
ROP	3.02×10^{-39}	1.39×10^{-39}	3.6×10^{-40}	4.77×10^{-39}
MEC	-	-	-	1.01×10^{-40}

TABLE III. Total integrated cross section predicted by the different RDWIA QE models and MEC. For the QE models, the contributions are separated by shells.

We show in Fig. 4 the cross section obtained from ED-RMF calculation, which considers the nuclear recoil. The different terms contributing to this results are separately shown. As illustrated in Fig. 3 and in Table II, the largest contribution in the p-shell region arises from the $1p_{3/2}$ state with a missing energy corresponding to the neutron separation of ¹²C, namely $E_m \approx 18.7$ MeV. In

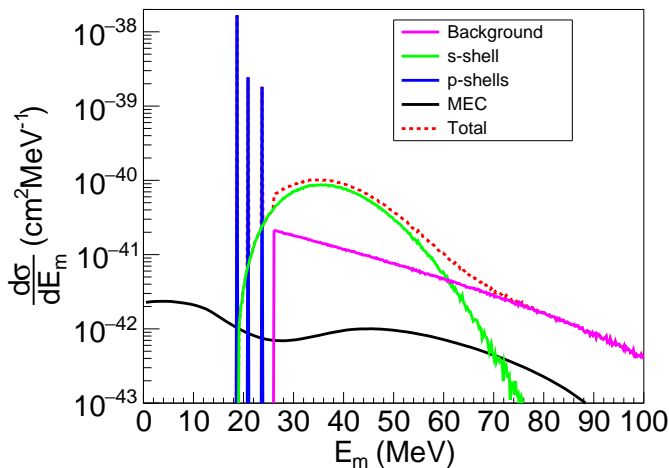


FIG. 4. Differential cross section as function of the missing energy separated by contributions of the different shells to the QE channel using the ED-RMF model with recoil. The contribution of MEC calculated with a semi-inclusive model based on the Relativistic Fermi gas [32, 33] is also shown separately.

contrast, the contribution of the neutrons from the s state is much broader, peaking at $E_m \approx 37.0$ MeV. The contribution of meson-exchange currents (MEC) is also shown separately in Fig. 4. This process corresponds to the emission of two nucleons induced by the coupling of the W -boson to the two-body MEC in the primary vertex. Its contribution to the cross section is calculated using a semi-inclusive model based on the Relativistic Fermi gas [32, 33]. The background and MEC contributions are significantly smaller and exhibit a broader distribution.

The relative importance of the various contributions can be more clearly assessed by examining the results reported in Table. III, where their integrated values are presented. The dominant contribution is that of the p -shell and that of the s is about half of it. The contribution of the background is one order of magnitude smaller, and even smaller is the contribution of MEC.

The comparison with the JSNS² experimental data requires two types of adjustments to our theoretical results. First, our cross section must be divided into bins of E_m . Second, a normalization procedure is necessary, since the JSNS² experiment provides only the shape of the cross section and not its absolute value.

The cross sections obtained after this procedure, calculated with the ED-RMF and ROP models, together with that obtained by implementing the ED-RMF results with the cascade simulation of NuWro, are shown in Fig. 5. The results of the upper panel include the nuclear recoil which is not considered in those of the lower panel.

In Fig. 5 the results of the ED-RMF and ROP calculations are very similar. This similarity arises from the common normalization applied to both results. Table. III presents the total contributions from the two calculations, showing that the total cross section predicted by

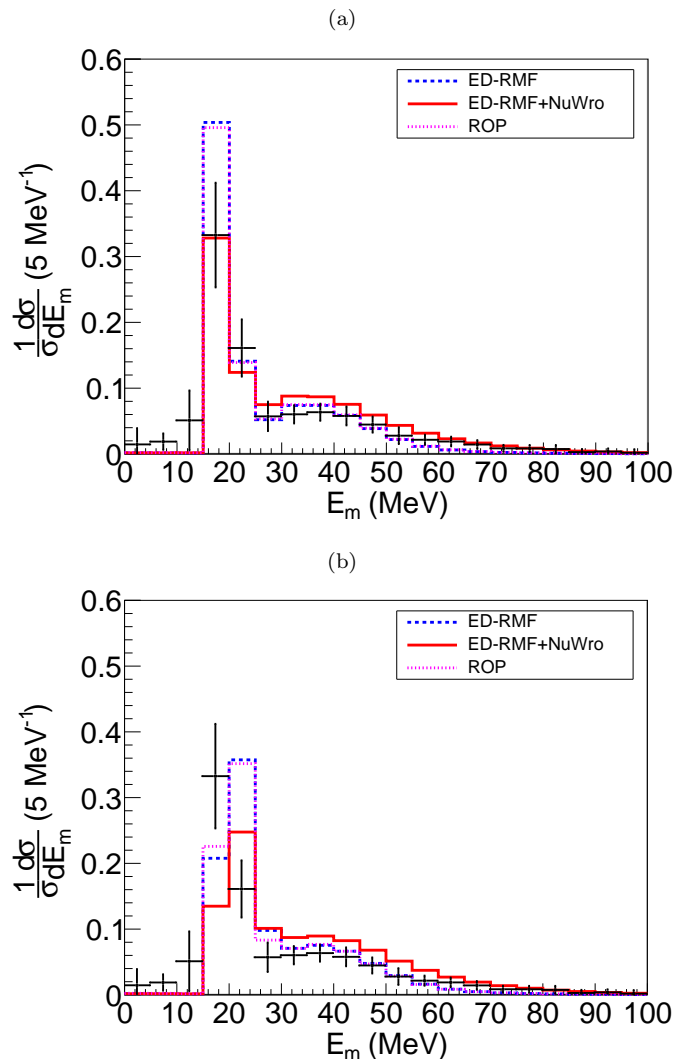


FIG. 5. Charge-current $\nu_\mu + {}^{12}\text{C}$ cross sections as a function of the missing energy E_m for an incoming neutrino with $E_\nu = 235.5$ MeV. All the theoretical results are normalized to the total strength of the experimental data. In the panel (a), the theoretical results consider the recoil of the residual nucleus in the definition of E_m . In the panel (b), this effect is neglected. All the results include both QE and MEC contributions.

the ROP model is about 27% smaller than that of the ED-RMF model. This is understandable, since the optical potential reduces the flux in the primary proton-emission channel, effectively redistributing it among other final-state channels.

The comparison between the results shown in the two panels clarifies the role of the residual-nucleus recoil. As already pointed out, neglecting this term in the evaluation of E_{vis} (see Eq. (18)) leads to an overestimation of the missing energy. In our calculations, this corresponds to a shift of approximately 1 to 5 MeV. As a consequence, when the recoil is not included, the p -shell peak appears in the $20 < E_m < 25$ MeV bin, as shown in the lower panel. If the recoiling residual nucleus does not produce

visible light in the detector, this effect could help explain the discrepancies observed between the data and the generator predictions, which does not account for recoil effects in the kinematics, in the region of the peak [3].

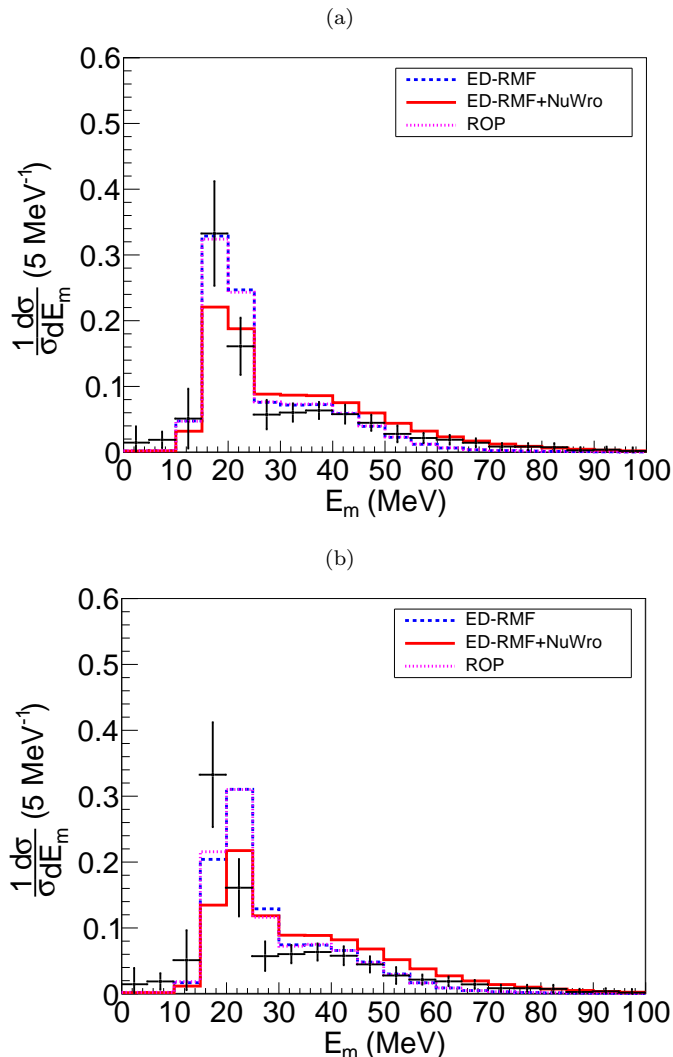


FIG. 6. Same than Fig. 5 but including a 2.5% energy smearing in the theoretical predictions.

The relevance of neutron emission is clearly illustrated in Fig. 5 by comparing the ED-RMF + NuWro results with those of the other calculations. The most prominent effect is the migration of events from the region dominated by the p -shells ($E_m < 22$ MeV) toward higher values of E_m , although the other shells are also affected by this mechanism. As a result, the ED-RMF + NuWro predictions overestimate the experimental data for $E_m > 30$ MeV in both cases presented in the figure, namely with and without including the recoil of the residual nucleus.

However, predictions from intranuclear cascade models for protons in the kinetic-energy range relevant to KDAR neutrinos must be interpreted with great care. Investigations of hadronic final-state interactions in neu-

trino–nucleus reactions have found substantial differences among different cascade-model predictions, and they also point to limitations of the semiclassical treatment at such low nucleon energies, where the Compton wavelength becomes comparable to the nuclear size [29, 34].

All the theoretical cross sections shown in Fig. 5 vanish below the neutron emission threshold of 18.7 MeV, as expected within our RDWIA models. However, the experimental data exhibit nonzero values even at energies below this threshold.

The presence of cross section below threshold may be attributed to nuclear structure effects, correlations, and also to the finite energy resolution of the detector. We simulate the detector smearing with a Gaussian distribution centered at E_{vis} and with a width $\sigma = 0.025 \times E_{\text{vis}}$. This 2.5% energy smearing is quoted in [3] to be a plausible estimate of the minimum energy resolution of the JSNS² detector.

The results obtained with this smearing procedure are shown in Fig. 6. We observe that the region below threshold is now populated by the theoretical cross sections, and the agreement with the experimental data is correspondingly improved.

VI. SUMMARY AND CONCLUSIONS

We analyzed the results of the JSNS² experiment [3], which observes charged-current (CC) interactions of muon neutrinos produced via kaon decay at rest (KDAR) on a ^{12}C target. In our model, the ν_μ interacts with a neutron in ^{12}C , which is converted into a proton via a CC interaction and subsequently emitted from the nucleus together with the associated μ^- .

The ^{12}C ground state is described within a relativistic mean-field model. In this framework, the nucleons in ^{12}C fully occupy the lowest single-particle levels, obtained by solving a set of coupled Dirac equations that include a potential simulating the average interaction of a nucleon with the remaining nucleons [4, 20]. The missing energy, E_m , takes discrete values corresponding to the single-particle level energies. Consequently, the missing-energy distribution $\rho_\kappa(E_m)$ consists of a sum of Dirac delta functions for all the occupied shells.

We improve this model by constructing a $\rho_\kappa(E_m)$ that reproduces the spectral function of Ankowski et al. [7]. Our $\rho_\kappa(E_m)$ parameterization consists of three contributions. The first is a sum of three delta functions accounting for the p -shell states. The second describes the s -shell contribution, modeled by a Maxwell–Boltzmann distribution. Finally, we include a background term that accounts for the effects of short-range correlations, which generate strength at large missing-energy values.

The final nuclear state, consisting of the emitted proton and the residual ^{11}C nucleus, is treated using three different approaches. In the first approach (ED-RMF), the proton wave function is distorted by the same real potential employed to describe the ^{12}C ground state. In

the second approach (ROP), the proton wave function is obtained by solving the Dirac equation with a complex optical potential. Finally, the ED-RMF wave function is used as input to the cascade model of NuWro, which simulates the re-scattering of the primary proton with the remaining nucleons within a semiclassical framework. This last modeling approach allows us to identify the role of neutron emission induced by re-scattering processes.

The comparison with the data is affected by an ambiguity in the definition of the missing energy, depending on whether the recoil of the residual nucleus is taken into account. We therefore present our results for both scenarios, namely with and without nuclear recoil. We find that including the recoil effect in our calculations leads to improved agreement with the experimental data, especially in the region of the p -shell peak. However, if JSNS² detector does not collect the light produced by the recoil, the shifted distribution obtained without the recoil could explain the inconsistencies found between the data and the generator predictions, which do not take into account the recoil in the kinematics, in the region of the peak.

The experimental data provide only the shape of the cross section as a function of the missing energy, not its absolute normalization. For this reason, all our results are normalized to the total strength of the empirical data. The ED-RMF and ROP calculations exhibit very similar profiles, although the overall strength of the ROP cross section is approximately 27% smaller than that of the ED-RMF result.

The situation is quite different for the ED-RMF + NuWro results. The shape of the distribution is modified, as part of the strength is shifted from the main p -shell contribution to larger missing-energy values. This effect arises from neutron emission induced by the re-scattering of the primary proton. Since the neutron energy is not detected by the JSNS² detector, the visible energy E_{vis} is reduced, consequently leading to a larger reconstructed missing energy (see Eqs. (17) and (18)). Including this mechanism leads to poorer agreement with the data, unlike the ED-RMF result. Ref. [34] compares proton-¹²C reaction cross-section with the predictions of different neutrino event generators and finds sizable discrepancies among the generators for $T_p < 30$ MeV, the kinematic region relevant for JSNS². Nevertheless, even when a generator reproduces the low- T_p reaction cross-section, the observable is inclusive and does not ensure an accurate modeling of particular inelastic final states,

such as channels involving neutron emission.

Another effect we have considered is the presence of cross section below the neutron-emission threshold. In our mean-field model, such contributions are forbidden. This discrepancy may arise from nuclear-structure effects not included in mean-field approaches, such as correlations, and/or from the finite energy resolution of the JSNS² detector. We simulate an energy smearing of the measured quantity E_{vis} with a Gaussian distribution centered at this value and width equal to 2.5% of E_{vis} . This procedure leads to an improved agreement with the experimental data.

The JSNS² experiment provides important insights into the nuclear-structure mechanisms underlying neutrino-nucleus interactions. Nevertheless, many questions remain open from both the experimental and theoretical viewpoints.

From an experimental perspective, the treatment of nuclear recoil energy remains ambiguous. Our results indicate that including recoil yields better agreement with the data than neglecting it. Yet the unfolding procedure of the data relies on a Monte Carlo event generator whose kinematics do not incorporate recoil. If the kinetic energy of the residual nucleus is not effectively detected, the generator would fail to describe the right position of the peak.

From the theoretical side, several issues remain to be addressed. For instance, the importance of low-energy collective excitations requires further investigation. In addition, low-energy p -¹²C reaction cross-section data suggest that the semi-classical description of inelastic FSI in cascade models might be inadequate in this energy regime.

The JSNS² experiment opens new opportunities in neutrino physics that deserve further investigation. In particular, measurements of absolute cross sections, beyond shape-only distributions, would be crucial to fully exploit the reach of these data.

ACKNOWLEDGMENTS

This work has been partially supported by INFN under Project NUCSYS. We would like to thank J. García-Marcos and R. González-Jiménez for propagating our theoretical predictions through NuWro and for useful discussions and V. Belocchi for providing the MEC calculation.

-
- [1] L. Alvarez-Ruso *et al.*, *Progress in Particle and Nuclear Physics* **100**, 1 (2018).
 - [2] A. A. Aguilar-Arevalo *et al.* (MiniBooNE Collaboration), *Phys. Rev. Lett.* **120**, 141802 (2018).
 - [3] E. Marzec *et al.* (JSNS² Collaboration), *Phys. Rev. Lett.* **134**, 081801 (2025).
 - [4] P. Ring, *Progress in Particle and Nuclear Physics* **37**, 193 (1996).
 - [5] J. Walecka, *Annals of Physics* **83**, 491 (1974).
 - [6] B. D. Serot and J. D. Walecka, Relativistic nuclear many-body theory, in *Recent Progress in Many-Body Theories: Volume 3*, edited by T. L. Ainsworth, C. E. Campbell, B. E. Clements, and E. Krotscheck (Springer US, Boston,

- MA, 1992) pp. 49–92.
- [7] A. M. Ankowski, O. Benhar, and M. Sakuda, *Phys. Rev. C* **110**, 054612 (2024).
- [8] J. M. Udías, P. Sarriguren, E. Moya de Guerra, E. Garrido, and J. A. Caballero, *Phys. Rev. C* **48**, 2731 (1993).
- [9] J. M. Udías, P. Sarriguren, E. Moya de Guerra, E. Garrido, and J. A. Caballero, *Phys. Rev. C* **51**, 3246 (1995).
- [10] J. M. Udías, J. A. Caballero, E. M. de Guerra, J. R. Vignote, and A. Escuderos, *Phys. Rev. C* **64**, 024614 (2001).
- [11] R. González-Jiménez, M. B. Barbaro, J. A. Caballero, T. W. Donnelly, N. Jachowicz, G. D. Megias, K. Niewczas, A. Nikolakopoulos, J. W. Van Orden, and J. M. Udías, *Phys. Rev. C* **105**, 025502 (2022).
- [12] A. Nikolakopoulos, R. González-Jiménez, N. Jachowicz, K. Niewczas, F. Sánchez, and J. M. Udías, *Phys. Rev. C* **105**, 054603 (2022).
- [13] J. M. Franco-Patino, R. González-Jiménez, S. Dolan, M. B. Barbaro, J. A. Caballero, G. D. Megias, and J. M. Udías, *Phys. Rev. D* **106**, 113005 (2022).
- [14] J. M. Franco-Patino, S. Dolan, R. González-Jiménez, M. B. Barbaro, J. A. Caballero, and G. D. Megias, *Phys. Rev. D* **109**, 013004 (2024).
- [15] T. Golan, C. Juszczak, and J. T. Sobczyk, *Phys. Rev. C* **86**, 015505 (2012).
- [16] K. Niewczas and J. T. Sobczyk, *Phys. Rev. C* **100**, 015505 (2019).
- [17] A. Nikolakopoulos, V. Pandey, J. Spitz, and N. Jachowicz, *Phys. Rev. C* **103**, 064603 (2021).
- [18] R. González-Jiménez, A. Nikolakopoulos, N. Jachowicz, and J. M. Udías, *Phys. Rev. C* **100**, 045501 (2019).
- [19] R. González-Jiménez, M. B. Barbaro, J. A. Caballero, T. W. Donnelly, N. Jachowicz, G. D. Megias, K. Niewczas, A. Nikolakopoulos, and J. M. Udías, *Phys. Rev. C* **101**, 015503 (2020).
- [20] M. Sharma, M. Nagarajan, and P. Ring, *Physics Letters B* **312**, 377 (1993).
- [21] H. De Vries, C. De Jager, and C. De Vries, *Atomic Data and Nuclear Data Tables* **36**, 495 (1987).
- [22] I. Angeli and K. Marinova, *Atomic Data and Nuclear Data Tables* **99**, 69 (2013).
- [23] M. Wang, W. Huang, F. Kondev, G. Audi, and S. Naimi, *Chinese Physics C* **45**, 030003 (2021).
- [24] E. D. Cooper, S. Hama, B. C. Clark, and R. L. Mercer, *Phys. Rev. C* **47**, 297 (1993).
- [25] O. Benhar, A. Fabrocini, S. Fantoni, and I. Sick, *Nuclear Physics A* **579**, 493 (1994).
- [26] O. Benhar, N. Farina, H. Nakamura, M. Sakuda, and R. Seki, *Phys. Rev. D* **72**, 053005 (2005).
- [27] G. Van Der Steenhoven, H. Blok, E. Jans, M. De Jong, L. Lapikás, E. Quint, and P. De Witt Huberts, *Nuclear Physics A* **480**, 547 (1988).
- [28] J. Mougey, M. Bernheim, A. Bussière, A. Gillebert, Phan Xuan Hô, M. Priou, D. Royer, I. Sick, and G. Wagner, *Nuclear Physics A* **262**, 461 (1976).
- [29] A. Nikolakopoulos, A. Ershova, R. González-Jiménez, J. Isaacson, A. M. Kelly, K. Niewczas, N. Rocco, and F. Sánchez, *Phys. Rev. C* **110**, 054611 (2024).
- [30] J. McKean, R. González-Jiménez, M. Kabirnezhad, J. M. Udías, and Y. Uchida, *Phys. Rev. D* **112**, 032009 (2025).
- [31] J. Garcia-Marcos, M. Hooft, T. Franco-Munoz, N. Jachowicz, J. M. Udías, K. Niewczas, A. Nikolakopoulos, and R. Gonzalez-Jimenez, (2025), [arXiv:2512.01721](https://arxiv.org/abs/2512.01721) [nucl-th].
- [32] V. Belocchi, M. B. Barbaro, A. De Pace, and M. Martini, *Phys. Rev. C* **109**, 065502 (2024), [arXiv:2401.13640](https://arxiv.org/abs/2401.13640) [nucl-th].
- [33] V. Belocchi, M. B. Barbaro, A. De Pace, and M. Martini, *Phys. Rev. D* **112**, 093002 (2025), [arXiv:2509.08786](https://arxiv.org/abs/2509.08786) [nucl-th].
- [34] S. Dytman, Y. Hayato, R. Raboanary, J. T. Sobczyk, J. Tena-Vidal, and N. Vololoniaina, *Phys. Rev. D* **104**, 053006 (2021).